Carpathian Journal of Earth and Environmental Sciences, February 2026, Vol. 21, No. 1, p. 155 – 170; DOI:10.26471/cjees/2026/021/360

SUPERCELL DYNAMICS AND TORNADOGENESIS IN THE VENETO REGION: SYNOPTIC AND MESOSCALE REANALYSIS OF THE 8 JULY 2015 *EF4* TORNADO

Jovan MIHAJLOVIĆ[1,2*] & Zorica VULOVIĆ[3]

[1]*Center for Climate Change, Institute for Interdisciplinary and Multidisciplinary Studies, University of Montenegro, Cetinjska br. 2, 81000 Podgorica, Montenegro; jovanm@ucg.ac.me*

[2]*Department of Geography, Faculty of Philosophy, University of Montenegro, Danila Bojovića bb., 81400 Nikšić, Montenegro; jovanm@ucg.ac.me*

[3]*Department of Tourism, Faculty of Geography, University of Belgrade, Studentski trg 3/III, 11000 Belgrade, Republic of Serbia; vulevac@gmail.com*

**Corresponding author: jovanm@ucg.ac.me*

Abstract: On 8 July 2015, a violent tornado rated *EF4* affected the Veneto region of northeastern Italy, causing severe impacts in a densely populated and culturally significant area. The event was officially documented in the European Severe Weather Database (ESWD) and represents one of the strongest tornadoes reliably recorded in the Mediterranean region. This study presents an integrated synoptic-to-local reanalysis of the atmospheric conditions associated with this event, combining reanalysis data, radiosonde observations, Doppler radar products, and satellite imagery. Results show that the tornado developed within a supercell thunderstorm embedded in a dynamically favorable environment characterized by strong vertical wind shear, pronounced atmospheric instability, and upper-level forcing associated with an approaching trough and jet-stream divergence. Mesoscale processes, including low-level convergence and orographic modulation by the Alpine barrier, played a key role in storm organization and intensification. Radar observations revealed classic supercell signatures, including a persistent mesocyclone and hook-shaped reflectivity, while satellite products indicated strong and sustained updrafts during the storm's mature phase. The findings demonstrate that, although rare, the Mediterranean environment can support intense tornadic supercells when synoptic forcing, mesoscale dynamics, and thermodynamic instability coincide. This case study contributes to a more comprehensive understanding of tornado-producing environments in southern Europe and provides insights relevant for regional hazard assessment, early-warning strategies, and risk awareness in areas with complex topography and high societal exposure.

Keywords: Mediterranean tornadoes, supercell thunderstorms, *EF4* tornado, Veneto, Doppler radar, satellite imagery, mesocyclone, MLCAPE, vertical wind shear

1. INTRODUCTION

Tornadoes – and their marine counterpart, waterspouts – though much less frequent than in classic Tornado Alley in the United States, are established phenomena in the Mediterranean basin, including Italy (Miglietta & Matsangouras, 2018). Over the period 2007 - 2016, a total of 371 tornadoes (TR) and 707 waterspouts (WS) were documented in Italy, indicating that such vortical storms are a non-trivial component of Italian severe-weather risk (Miglietta & Matsangouras, 2018). This dataset reveals an average annual rate of approximately 32 land tornadoes and 49 waterspouts, albeit with considerable interannual variability (Miglietta & Matsangouras, 2018; ECSS, 2017).

Spatially, tornado and waterspout occurrences are not evenly distributed across Italy. The highest densities are found along coastal areas and in flat, low-lying plains: the Venetian plain, parts of the Po Valley and Friulian plain, Tyrrhenian and Ionian coasts, and southern regions including Apulia and Sicily (Miglietta & Matsangouras, 2018; Giaiotti et al., 2007). These "hotspots" emerge from the interplay of Mediterranean moisture, orographic and coastal effects, and synoptic-scale forcing favorable

to severe convection (Miglietta & Matsangouras, 2018; Avolio & Miglietta, 2023).

Italian tornadoes are statistically weaker than their U.S. counterparts: in the long-term climatologies, the majority of events are rated *F0–F2*, with only a small fraction reaching *F3* or stronger (Giaiotti et al., 2007; Miglietta & Matsangouras, 2018). This statistical distribution reflects the generally lower convective available potential energy (CAPE) and milder thermodynamic contrasts typical of the Mediterranean climate (Giaiotti et al., 2007). Nonetheless, rare but violent tornadoes have struck – especially in northeastern Italy – and when they hit densely built or historically significant areas, the consequences may be severe.

Important historical examples include the Tromba del Montello of 24 July 1930, widely regarded as the strongest tornado ever documented in Italy. This multivortex event – covering a path of some 60 - 80 km in northeastern Italy – caused widespread destruction, with reported peak intensity equivalent to *F5* on the Fujita scale, around 23 fatalities, and over a hundred injured (Pipinato, 2018). The Montello event remains a sobering reminder that the Mediterranean is not immune to tornadoes of catastrophic strength.

More recent data continue to underscore significant risk. A climatological reassessment revealed that over the three decades 1990 - 2021, hundreds of *EF1+* tornadoes occurred in Italy, with two regions – the central Tyrrhenian and southeastern Apulia – identified as especially active "Mediterranean tornado hotspots" (Avolio & Miglietta, 2023). Analysis of radiosonde observations, reanalysis data (e.g., ERA5), and large-scale atmospheric patterns suggest that the combination of moisture-rich low-level flow, vertical wind shear, and synoptic forcing (e.g., troughs, Mediterranean cyclones) often primes the atmosphere for tornadogenesis (Avolio & Miglietta, 2023; Bagaglini et al., 2021).

In this context, the event that struck the Riviera del Brenta (towns of Mira, Dolo and Pianiga) on 8 July 2015 is of particular interest. Although formally a rare occurrence, the 2015 tornado caused extensive structural damage and impacted a densely inhabited and culturally rich area, underscoring the vulnerability of northern-Italian plains to tornadic storms even in the absence of "classic" U.S.-style supercell conditions. The case highlights how, under favorable mesoscale and synoptic conditions, the Mediterranean environment can produce concentrated, high-impact tornadoes – a concern that remains under-studied (Pipinato, 2018).

From a risk-assessment and hazard-mitigation perspective, detailed studies of such events are essential. First, each strong Italian tornado adds valuable data for refining Mediterranean tornado climatology, improving statistical risk estimates and spatial hazard maps (Miglietta & Matsangouras, 2018; Avolio & Miglietta, 2023). Second, understanding how local building typologies – especially historical masonry structures and villas typical of Venetian plains – respond to tornadic winds is crucial for forensic analysis, reconstruction, and future resilience planning (Zanini et al., 2017; Pipinato, 2018). Third, comprehensive synoptic-to-local reconstructions (combining reanalysis, radar, and damage-survey data) can shed light on the meteorological precursors and mechanisms of tornadogenesis in complex Mediterranean settings, informing early-warning efforts and civil protection strategies (Bagaglini et al., 2021; Avolio & Miglietta, 2023).

Despite the growing body of research, significant gaps remain. The climatological databases are incomplete, partly due to underreporting – many tornadoes likely go undocumented in rural or sparsely monitored areas (Giaiotti et al., 2007; ECSS, 2017). The structural-damage literature for Mediterranean building types remains limited (Pipinato, 2018; Zanini et al., 2017). And the linkage between reanalysis-based atmospheric diagnostics and actual observed damage is not yet systematically established for many events.

However, the key research gap is that high-resolution, multi-method analyses of Mediterranean tornadoes, particularly strong *EF3–EF4* events, remain extremely scarce. Previous studies have typically addressed either synoptic or mesoscale conditions, radar signatures, or historical climatology in isolation, without integrating reanalysis data, radiosonde observations, satellite imagery, radar, and ESWD documentation.

The present study addresses this gap by providing an integrated, multi-method reconstruction of the 8 July 2015 *EF4* tornado in the Veneto region. This is the first time such a comprehensive approach has been applied to a high-impact Mediterranean tornado in this area, where the complex Alpine orography and land-sea interactions critically influence convective evolution. By linking environmental conditions, mesoscale storm dynamics, and observed tornado intensity, this study advances previous Mediterranean tornado research and provides novel insights for hazard assessment and early-warning planning.

Given the complex meteorological setting of the Veneto region and the broader Mediterranean, tornado occurrence remains relatively rare but can result in disproportionately high impacts due to population density, cultural heritage, and

infrastructure vulnerability (Dotzek et al., 2003; Trapp et al., 2007; Antonescu et al., 2016). Previous studies have highlighted the role of synoptic-scale cyclones, upper-level troughs, and localized mesoscale instability in producing severe convective storms in Southern Europe (Doswell et al., 1996; Brooks et al., 2003; Antonescu & Schultz, 2016), while analyses of individual Mediterranean tornado events have emphasized the influence of topography, land-sea contrasts, and mesoscale convective boundaries (Picca et al., 2010; Delobbe et al., 2013; Romero et al., 2018). Despite these insights, systematic high-resolution case studies integrating synoptic, mesoscale, and radar-based evidence remain limited, particularly in regions with dense urban and heritage assets where accurate hazard assessment is critical (Tsanis et al., 2003; Holzer et al., 2011; Antonescu et al., 2018).

2. DATA SOURCES AND RESEARCH METHODOLOGY

The analysis of the 8 July 2015 tornado in the Veneto region is based on a combination of synoptic-scale (large-scale atmospheric patterns), mesoscale (regional weather features), radar, satellite, and upper-air (radiosonde) datasets (see Table 1). These sources were selected to provide a comprehensive reconstruction of the atmospheric environment, capturing both large-scale forcing and mesoscale instability, as well as storm-scale characteristics associated with tornado formation. Diagnostic variables derived from these datasets include vertical vorticity, wind shear (changes in wind speed and direction with height), divergence (air spreading aloft), vertical velocity (upward motion in the atmosphere), and various instability indices, including Convective Available Potential Energy (CAPE), Lifted Index (LI), Storm-Relative Helicity (SRH), Energy-Helicity Index (EHI), Supercell Composite Parameter (SCP), and Significant Tornado Parameter (STP – quantifies the likelihood of tornadic supercell development using wind shear and instability metrics). Each of these metrics provides insight into the potential for strong rotating thunderstorms and tornadoes. Tornado intensity was assessed using the Fujita (*F*) and Enhanced Fujita (*EF*) scales, which classify tornadoes based on observed wind speeds and associated effects.

To quantify the kinematic and thermodynamic environment, only the key equations used in the analysis are presented. These represent the quantities directly computed for assessing tornado potential (see Table 2).

Table 1. Data sources.

Dataset	Provider / Institution	Product Type	Notes / Resolution
GFS (Global Forecast System)	NOAA/NCEP	Synoptic and mesoscale forecasts	0.25°, 00/06/12/18 UTC
METEOSAT Second Generation (MSG)	EUMETSAT	Satellite imagery	Infrared, Water Vapor, and Visible channels
Radar composites	ARPAV Veneto	Radar reflectivity and velocity	Volumetric scans
Upper-air soundings	University of Wyoming / Local sounding archive	Radiosonde profiles	00/12 UTC; used to derive hodographs and vertical profiles
Synoptic charts	Wetter3	Surface and upper-air analyses	Multiple levels
Mesoscale analyses	WeatherOnline	Composite mesoscale fields	High-resolution maps

Note: All datasets are publicly available and were accessed in accordance with the respective providers' data policies.

Synoptic- and mesoscale analyses were derived from the Global Forecast System (GFS) model outputs, which provide large-scale atmospheric patterns and regional weather features useful for reconstructing the environmental conditions leading to the tornado. Tornado tracks and terrain profiles were created using GPS Visualizer, while radar and satellite imagery were processed using PhotoScape and Microsoft Office Picture Manager. Hodographs and vertical profiles from radiosonde data were computed using standard processing routines.

2.1. Data Limitations and Uncertainty Assessment

While the multi-source observational framework employed in this study allows for a detailed reconstruction of the 8 July 2015 tornado event, several limitations and sources of uncertainty should be acknowledged. Doppler radar coverage over northeastern Italy is constrained by beam-height increase with distance and partial shielding by complex terrain, which may limit the detection of low-level rotational features at greater ranges. As a result, the precise vertical extent and intensity of the mesocyclone near the surface may be underestimated.

Radiosonde observations are spatially limited and do not coincide exactly with the location or timing of tornadogenesis. Although nearby soundings

Table 2. Key diagnostic equations used to assess tornado potential and term definitions.

Equation	Description	Terms
$\zeta = \frac{\partial v}{\partial x} - \frac{\partial u}{\partial y}$	Vertical component of vorticity	u,v: horizontal wind components
$CAPE = \int_{LFC}^{LNB} g \frac{\theta_{v,p} - \theta_{v,e}}{\theta_{v,e}} dz$	Convective Available Potential Energy, representing the buoyant energy available to a rising parcel	$\theta_{v,p}$: virtual potential temperature of parcel; $\theta_{v,e}$: virtual potential temperature of environment; *LFC*: Level of Free Convection; *LNB*: Level of Neutral Buoyancy; g: gravity
$SRH = \int_0^h k \cdot (\vec{V} - \vec{C}) \cdot (\nabla \times V)\, dz,$	Storm-Relative Helicity for a layer of depth h	$\vec{V}$: horizontal wind vector; $\vec{C}$: storm motion vector; h: layer depth (typically 0-3 km)
$EHI = \frac{CAPE \cdot SRH}{C_0}$	Energy-Helicity Index, combining instability and helicity	C_0: empirical constant; *CAPE* and *SRH* as above
$SCP = \frac{MUCAPE}{1000} \cdot \frac{SRH_{0-3}}{50} \cdot \frac{BRN}{40}$	Supercell Composite Parameter, integrating CAPE, helicity, and storm balance	*MUCAPE*: mixed-layer CAPE; SRH_{0-3}: 0-3 km storm-relative helicity; *BRN*: Bulk Richardson Number
$STP = f(CAPE, SHR, LCL, shear)$	Significant Tornado Parameter (modified), combining instability, shear, and boundary-layer properties	*CAPE*: convective available potential energy; *SRH*: storm-relative helicity; *LCL*: lifted condensation level; *shear*: low-level vertical wind shear

provide a representative depiction of the pre-convective environment, small-scale thermodynamic and kinematic variability cannot be fully resolved. Similarly, reanalysis datasets, while valuable for synoptic and mesoscale diagnostics, may smooth localized extremes relevant to severe convection.

Uncertainty also exists in post-event intensity estimation, which relies on available observational evidence and established forensic methodologies. While the *EF4* classification is supported by multiple lines of evidence, including documented impacts and storm characteristics, inherent uncertainties remain due to the localized and transient nature of tornado damage and atmospheric processes.

Despite these limitations, the convergence of independent observational datasets provides a consistent and physically coherent depiction of the atmospheric conditions associated with this event, supporting the robustness of the main conclusions.

3. RESEARCH RESULTS

3.1. Synoptic Analysis – Surface and Upper-Level Atmospheric Structure

On 8 July 2015, the surface synoptic situation over Europe was characterized by a complex pressure pattern (Figure 1a). A mature occluded cyclone was located south of Greenland and west of the British Isles, bringing a cold front that advected cool air over the entire cyclone area and caused local pressure increases due to the displacement of cold air. South of this system, a broad high-pressure area with a 1025 mb isobar was present, which later expanded to form a secondary high-pressure field as it moved toward the Brittany Peninsula and the British Isles. The ridge associated with this anticyclone intensified, displacing frontal systems toward the Alps and enhancing regional atmospheric instability. Over the Iberian Peninsula and along the Mediterranean, weak secondary cyclonic and anticyclonic centers were present. In the North Sea, between the British Isles and Norway, another occluded cyclone with associated frontal systems was observed; this system gradually became thermally stable and weakened due to surface friction, leading to the eventual dissipation of its circulation.

Two frontal systems were particularly influential in producing the tornado over Northern Italy. The first was associated with the occluded North Sea cyclone, while the second extended parallel to the first from the Iberian Peninsula, across the Gulf of Genoa, the Alps, Central Europe, and into Russia and Ukraine. At 06 UTC, a small cyclonic center formed in the Gulf of Gdańsk as a result of convergence lines and a high-pressure center over Poland, which distorted the frontal wave. Orographic interaction with the Alpine chain and the mountainous regions of Central Europe slowed and deformed the frontal system, generating a quasi-stationary front. Along this boundary, a strong horizontal temperature gradient and cold-air accumulation on the upstream side of the orography led to enhanced winds and cold advection around the mountain system, increasing the surface pressure

gradient. This quasi-stationary instability zone favored the development of successive thunderstorms (training storms) as the convective line interacted with warmer surrounding air. Additional intrusion of cold air around the Alps increased cyclonic vorticity and promoted the formation of closed cyclonic circulation. Between 12 and 18 UTC, a low-pressure center formed over the Po Valley, closed by the 1005 mb isobar.

At 500 mb (Figure 1b), absolute geopotential height and temperature analyses revealed a prominent upper-level anticyclone centered over Madeira, with a ridge extending across the Iberian, Apennine, and Balkan peninsulas, reaching the Azores and Ural region. This induced subsiding motion of warmed air into the lower troposphere, contributing to destabilization in regions where surface heating was strong. The upper-level trough associated with a cyclone over the Barents Sea extended from the British Isles across Brittany, France, and the Bay of Biscay, providing a channel for cold-air advection from the north. As this trough axis migrated eastward from 12 to 18 UTC, it crossed Northern Italy, further promoting subsidence and vertical destabilization in the lower atmosphere.

At 300 mb (Figure 1c), the jet stream axis was located slightly north of Italy, along the frontal zone, with peripheral wind speeds of 60 - 85 knots and over 100 knots along the core. This configuration produced strong vertical wind shear necessary for supercellular rotation. A pronounced horizontal field of positive divergence was observed above the Gulf of Trieste, sustained by the jet's kinetic energy. This upper-level divergence induced surface convergence, creating favorable conditions for tornado development.

In summary, the synoptic analysis indicates that the three principal conditions for tornado formation were satisfied on 8 July 2015 over Northern Italy:

1. Presence of a surface low-pressure center over the Po Valley;
2. An upstream upper-level trough providing cold-air advection and subsidence;
3. A 300 mb jet stream creating a divergent field and enhancing vertical wind shear across the atmospheric column.

These conditions collectively created a highly favorable environment for the development of tornadic supercell convection in the region.

3.2. Mesoscale Analysis of the Weather Situation

To more precisely identify the meteorological factors that contributed to the development of the supercell and tornado in the Veneto region, a mesoscale analysis was conducted using high-resolution diagnostics. The mesoscale fields examined include:

(1) surface pressure (hPa);
(2) surface pressure tendency (hPa/3 h);
(3) wind at 10 m, 850 hPa, 700 hPa, and 500 hPa;
(4) vorticity advection at 850 and 500 hPa;
(5) mixed-layer CAPE (MLCAPE – Mixed-Layer Convective Available Potential Energy, a measure

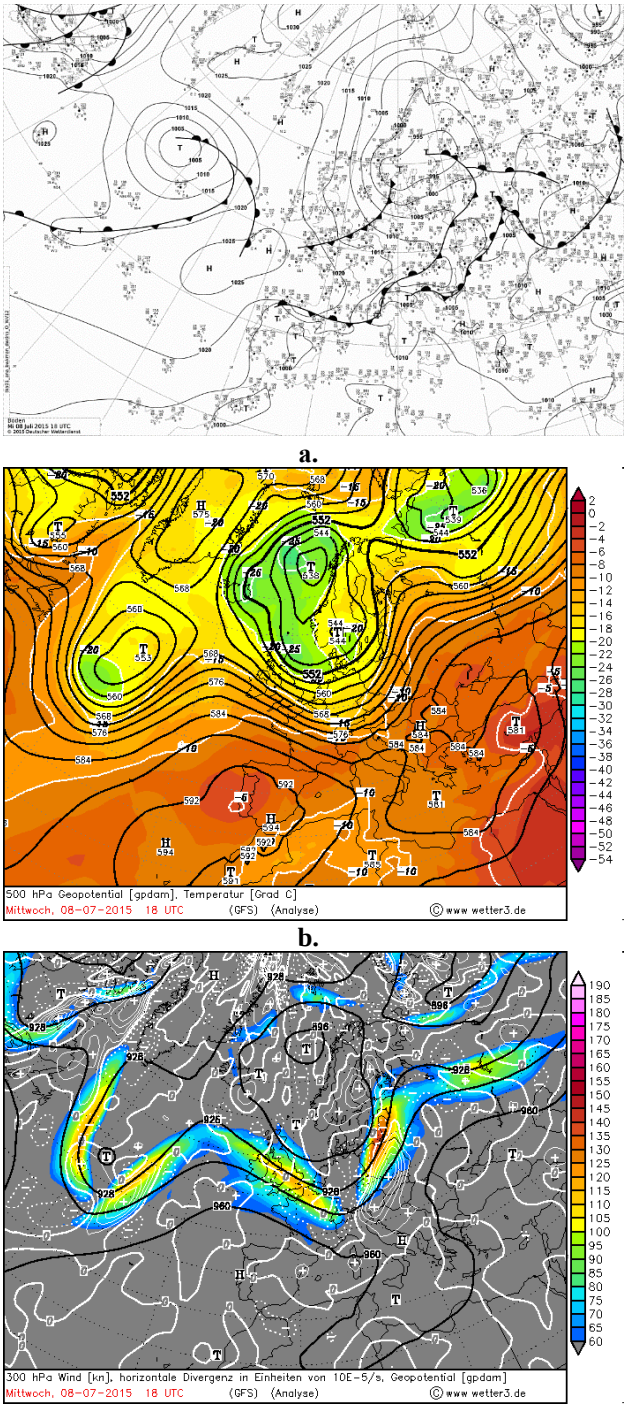

Figure 1. Synoptic surface analysis (a), 500-mb analysis chart (b), and 300-hPa wind field (c) over Europe on 8 July 2015 at 18 UTC.

of the energy available for upward motion in thunderstorms).

One of the key synoptic precursors for tornadogenesis is the presence of an upper-level trough positioned west of the tornado location, capable of enhancing surface cyclogenesis. Analysis of the surface pressure charts shows that between 15 and 18 UTC a closed low-pressure area of approximately 1006 hPa was present, deepening to 1005 hPa by 18 UTC – consistent with the timing of tornadogenesis in the Veneto region. At 18 UTC, the axis of the surface trough is clearly defined over the area in which the supercell initiated. The mesoscale pressure-tendency chart at 15 UTC indicates a pressure fall of -6 to -10 hPa per 3 hours (Figure 2a, b).

Wind at 10 m (18 UTC) blows from the SW–SE at 15 - 25 kt, indicating a weakly convergent boundary-layer flow. At 850 hPa, a cyclonic rotation is evident, with winds from the west at 25 - 30 kt. At 700 hPa, the flow is from the W-SW at around 30 kt. By 500 hPa, wind direction shifts again, blowing from W–SW–NW at 35 - 55 kt. These features collectively point to strong vertical wind shear in both speed and direction – a critical ingredient for supercell development.

Positive values of vorticity advection at both 850 and 500 hPa between 15 and 18 UTC indicate sufficient dynamical forcing to sustain upward motion and enhance storm-scale rotation. High MLCAPE values ($2200\,Jkg^{-1}$), together with low Lifted Index values ($-6\,K$), observed at 12 UTC, reveal substantial thermodynamic instability over the Gulf of Trieste and the Po Valley in the hours preceding supercell initiation (Figure 3a, b).

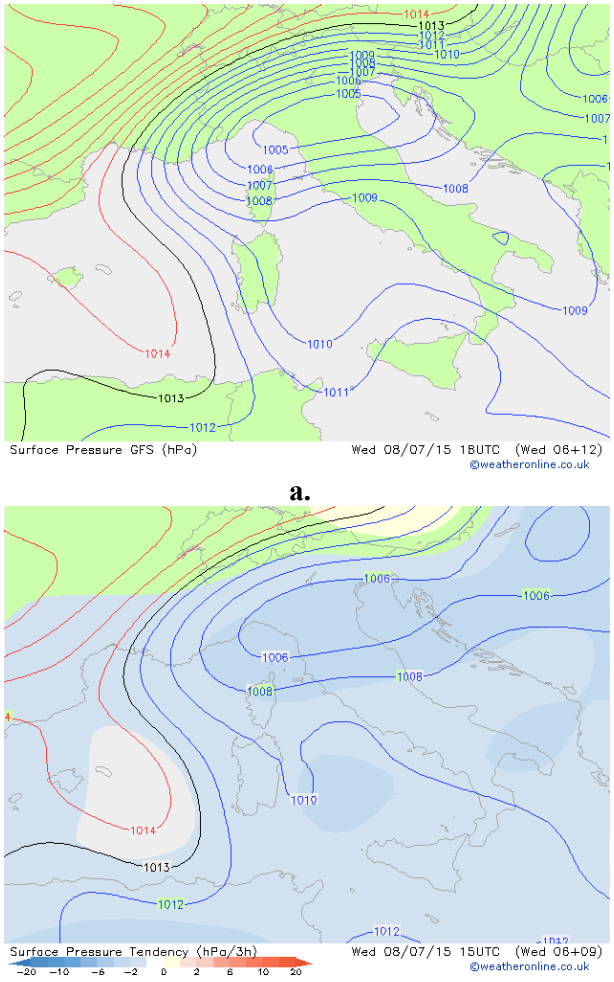

Figure 2. Surface pressure (hPa) and surface pressure tendency (hPa/3 h) over the broader Apennine region on 8 July 2015, shown for 18 UTC (a) and 15 UTC (b).

3.3. Radiosonde Diagnostics and Hodograph-Based Kinematic Assessment

Radiosonde profiles and hodographs were examined for the stations Udine (16044) (Figure 4a) and San Pietro Capofiume (16144) (Figure 4b) on 8 July 2015 at 00 UTC. Because no 12 UTC sounding was launched from these stations on the day of the event, the 12 UTC profile from Milan (16080) (Figure 6), located 245.77 km from Venice in a straight line, was used as a substitute.

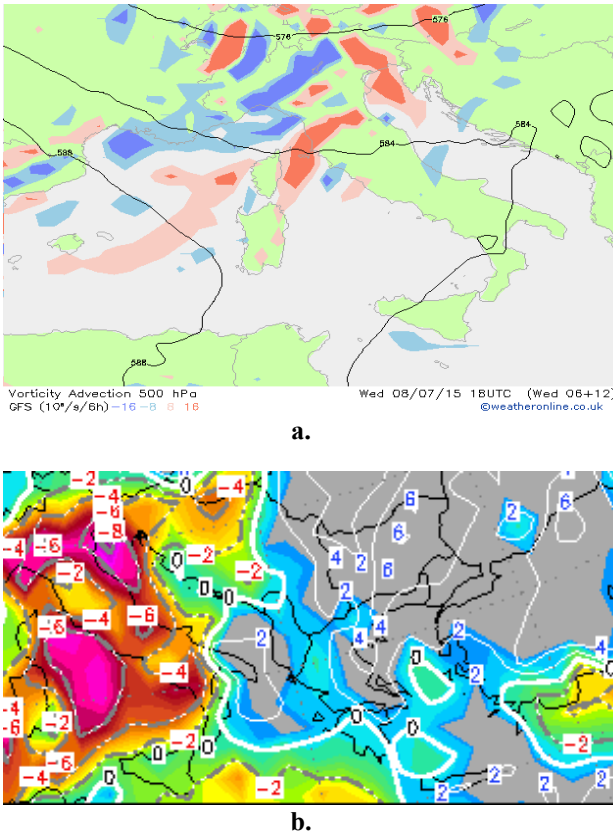

Figure 3. Vorticity advection at 500 hPa (a) and MLCAPE (b) over the broader Apennine region on 8 July 2015 at 18 UTC.

The vertical thermodynamic profiles for all three stations indicate that the atmosphere was conditionally to near-adiabatically unstable from approximately 700 mb upward, with substantial convective instability. The lower troposphere was nearly saturated up to about 800 mb, and dew-point temperatures ranged from 15 °C to over 20 °C near the surface. The wind profiles exhibit strong speed and directional shear: southwesterly flow dominated the boundary layer, westerly winds prevailed around 600 - 500 mb, the flow veered again to southwesterly near 500 mb, and returned to westerly at 300 mb. Wind speeds increased sharply above 500 mb, indicating intense upper-level flow, and at 300 mb the profile reflects the presence of the jet stream.

Parcel temperatures exceeded environmental temperatures through a deep layer, indicating positive buoyancy, while the lapse rate between 850 and 600 mb (≈ 20.03 °C) was sufficiently steep to support convective initiation. The 00 UTC sounding indicates environmental conditions favorable for scattered to severe thunderstorms, multicell convection, large hail, and tornado potential. The LCL (AGL) was 113.13 m, and the equilibrium level was located at 13.32 km. The convective temperature was 35.59 °C, and the freezing level height was 4536 m ($H_{-10} = 6024\ m$), supporting the potential for hailstones up to approximately 5.3 cm in diameter. Large values of MLCAPE ($CAPE = 2809\ Jkg^{-1}, \rightleftarrows\ CAPE\ Virt = 3009\ Jkg^{-1}$), (Figure 5) together with a lifting index ($LI = -6.80$ °C), further confirm the high degree of instability. Updraft kinetic energy implied maximum vertical velocities on the order of 75 - 78 m s^{-1}, consistent with very strong or extreme updraft potential. The downdraft (negative buoyancy) energy was also substantial $-DCAPE = 1082\ Jkg^{-1}$, and from the height of maximum in-cloud vertical velocity (5890 m), downdraft speeds (w_{max}) of approximately 47 ms^{-1} could be generated. Instability parameters yielded values of (SI = -6.98 °C; MTI = 44.60 °C; TT index =56 °C; KO = -13.07; SWISS 12 = -8.44) indicating potential for scattered to strong convection. The Significant Tornado Parameter (STP) was 0.69, consistent with some tornado potential, while the Derecho Composite Parameter of 1.03 indicated the possibility of widespread severe winds. Wind-related parameters further show storm-relative winds of 16.74 kt in the 9 - 11 km layer and confirm the presence of upper-level jet influence. The 3-km Vorticity Generation Potential (0.16 s^{-1}) suggests a favorable environment for tornadogenesis. The Udine sounding showed comparable wind characteristics, though the storm-relative winds in the 9 - 11 km layer (16.93 kt) suggested potential for HP (high-precipitation) supercell development.

The 12 UTC Milan sounding indicated a supercell motion vector of 21.40 kt. Storm-relative winds from the surface to 2 km were 17.88 kt, and in the 9–11 km layer reached 27.91 kt, demonstrating strong deep-layer shear supportive of tornadic supercells. Effective bulk shear reached 42.70 kt, and BRN shear was 28.75, indicative of an environment capable of supporting multicellular convection. Low-level helicity within the 0 - 3 km layer was 140.06 $m^2\ s^{-2}$ supporting supercell development, while an EHI value of 2.46 indicated a non-negligible probability of mesocyclone-driven tornadogenesis.

3.4. Satellite-Derived Top-Down Analysis of Storm Structure and Evolution

Satellite-based analysis was performed using imagery from the second-generation geostationary METEOSAT platform, which provides continuous, high-temporal-resolution observations of cloud development and atmospheric processes over Europe. Satellite products are particularly valuable for monitoring convective storms because they allow early identification of rapidly growing cloud tops, strong updrafts, and storm organization over large areas where in situ observations may be sparse.

Multiple spectral composites were analyzed, including Airmass RGB, Dust RGB, Natural Color RGB, High-Resolution Visible (HRVIS), and Severe Storm RGB products. The Severe Storm RGB composite highlights regions of strong vertical development and intense convection by combining information from water vapor and infrared channels, making it especially useful for identifying potentially severe thunderstorms. These products were used to assess cloud-top height, vertical growth rate, and the presence of overshooting tops, which are indicative of vigorous updrafts and dynamically strong convective cells.

The satellite observations revealed high, dense, ice-laden cloud tops and pronounced overshooting features, consistent with deep, sustained updrafts typically associated with supercell storms. Such satellite signatures are widely recognized as early indicators of severe convective potential and often precede radar-detected supercell structures and tornado formation.

Satellite imagery (12 UTC) from the Meteosat Second Generation (MSG) geostationary satellites indicates the presence of convective cloudiness over northern Italy and its surroundings, fully consistent with the synoptic situation on the day of the event. METEOSAT-10, positioned at 0° longitude, is the primary operational geostationary platform, providing full-disc imagery every 15 minutes

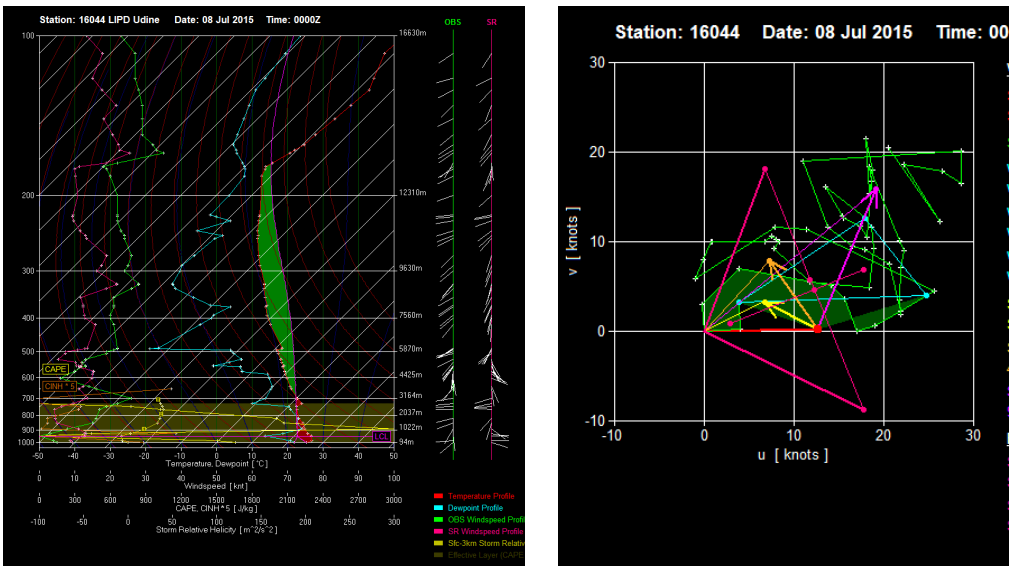

a.

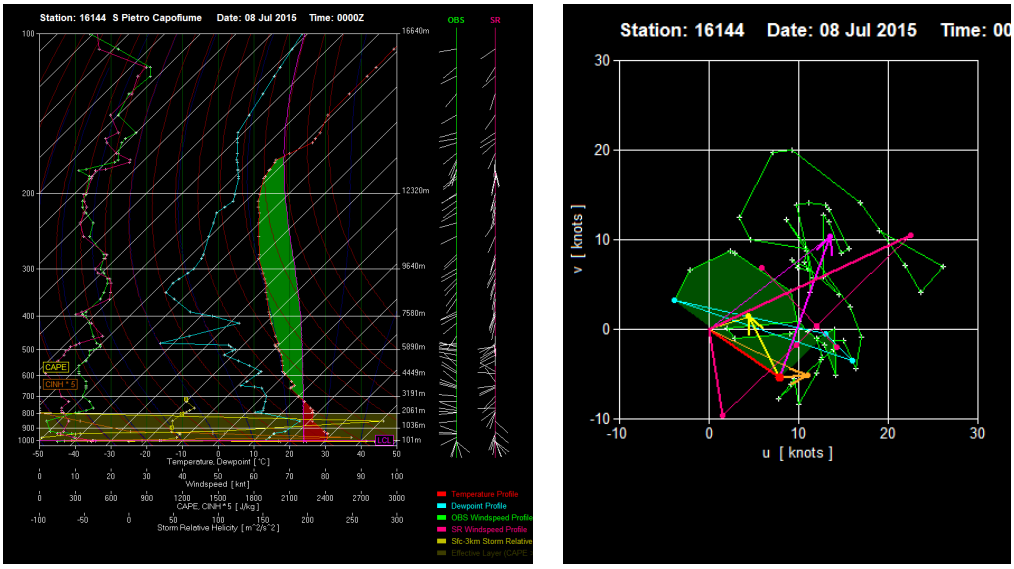

b.

Figure 4. Skew-T log-P diagrams and wind hodographs for the Udine (a) and San Pietro Capofiume (b) stations on 8 July 2015 at 00 UTC.

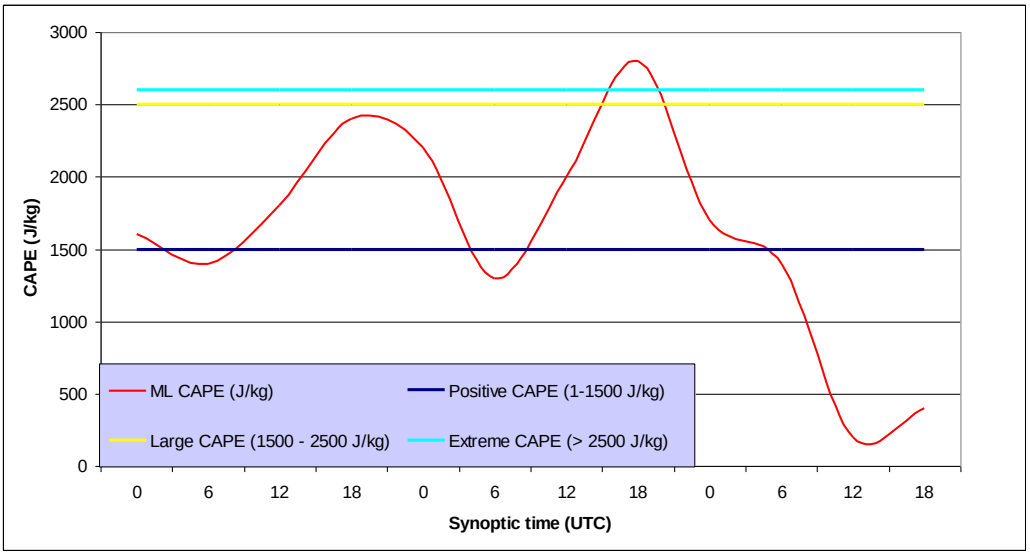

Figure 5. Values of MLCAPE (J kg^{-1}) at the main synoptic times.

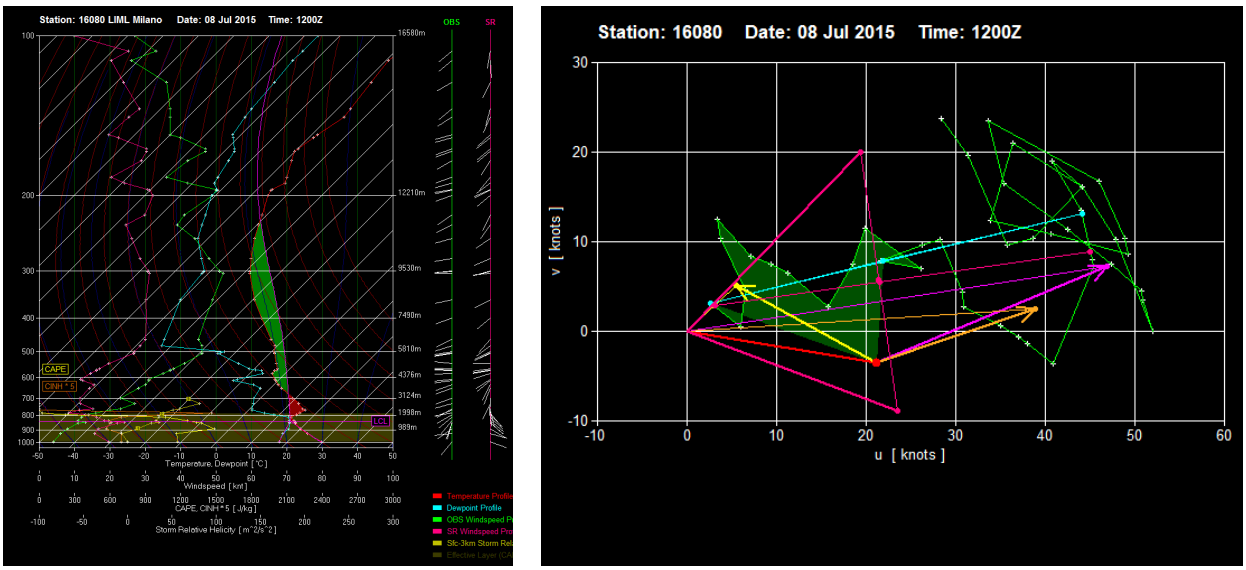

Figure 6. Skew-T log-P diagram and wind hodograph for the Milan station on 8 July 2015 at 12 UTC.

METEOSAT-9 operates in rapid-scanning mode, delivering imagery every 5 minutes over selected regions of Europe, Africa, and adjacent seas. METEOSAT-8 functions as a backup for both satellites, while METEOSAT-7 (launched in 1997), the last of the first-generation Meteosat satellites, monitors the Indian Ocean region (www.eumetsat.int). The MSG constellation is essential for detection, nowcasting, and detailed monitoring of convective processes that lead to severe thunderstorms, as well as for assessing air-mass characteristics up to six hours in advance.

The following RGB composites were analyzed at 12 UTC: Airmass RGB, Day Microphysics RGB, Dust RGB, HRVIS RGB, Natural Colour RGB, and Severe Storm RGB, as illustrated in Figure 7a-f.

The Airmass RGB (Figure 7a) highlights the presence of high, opaque cloud tops depicted in white tones. The developing convective cell (a nascent supercell) is identifiable primarily by its characteristic shape rather than by color. Red hues on the composite indicate a hot and dry air mass south of the Alps, whereas the environment surrounding the Alpine range and the storm system is marked by high upper-tropospheric humidity – conditions that are conducive to tornadogenesis. In the Day Microphysics RGB (Figure 7b), deep convective clouds appear in orange shades, indicative of small ice crystals associated with strong updrafts and the rapid intensification of the supercell. The Dust RGB (Figure 7c) portrays high, opaque cloud tops in red tones. On the HRVIS RGB composite (Figure 7d), the supercell's anvil and high opaque cloud cover are represented by various shades of blue. In the Natural Colour RGB (Figure 7e), cold, ice-rich clouds – corresponding to cumulonimbus tops, including the supercell – appear in cyan hues. Finally, the Severe Storm RGB (Figure 7f) displays thick ice clouds in red and yellow tones. Because the supercell was still in its formative stage, its cloud tops had not yet reached very low temperatures (deep red colors). The brighter tones near the storm top indicate an intense updraft and an early phase of vertical development. This composite is particularly valuable for identifying the most active regions within the convective system.

3.5. Doppler Radar Signatures and Mesocyclone Detection

The radar analysis revealed a hook echo, a characteristic curved reflectivity pattern typically associated with rotating supercell storms, as well as a Weak Echo Region (WER) and Bounded Weak Echo Region (BWER), which indicate the presence of strong and persistent updrafts capable of supporting severe weather.

The supercell thunderstorm that produced the Mira (Venice) tornado on 8 July 2015 was observed by the ARPAV meteorological radar located at the Monte Grande di Teolo radar center (Padua). Radar echoes over the affected region were analyzed using two corrected-intensity radar products:

1. BASE Section Corrected Intensity (dBZ);
2. PPI 1.5° Corrected Intensity (dBZ).

In addition, vertical cross-sections were extracted along selected azimuths from the PPI 1.5° product for time steps between 09:30 UTC and 16:10 UTC. These radar datasets capture both the initial development and the peak intensity of the supercell, revealing reflectivity structures characteristic of a mature, rotating convective storm.

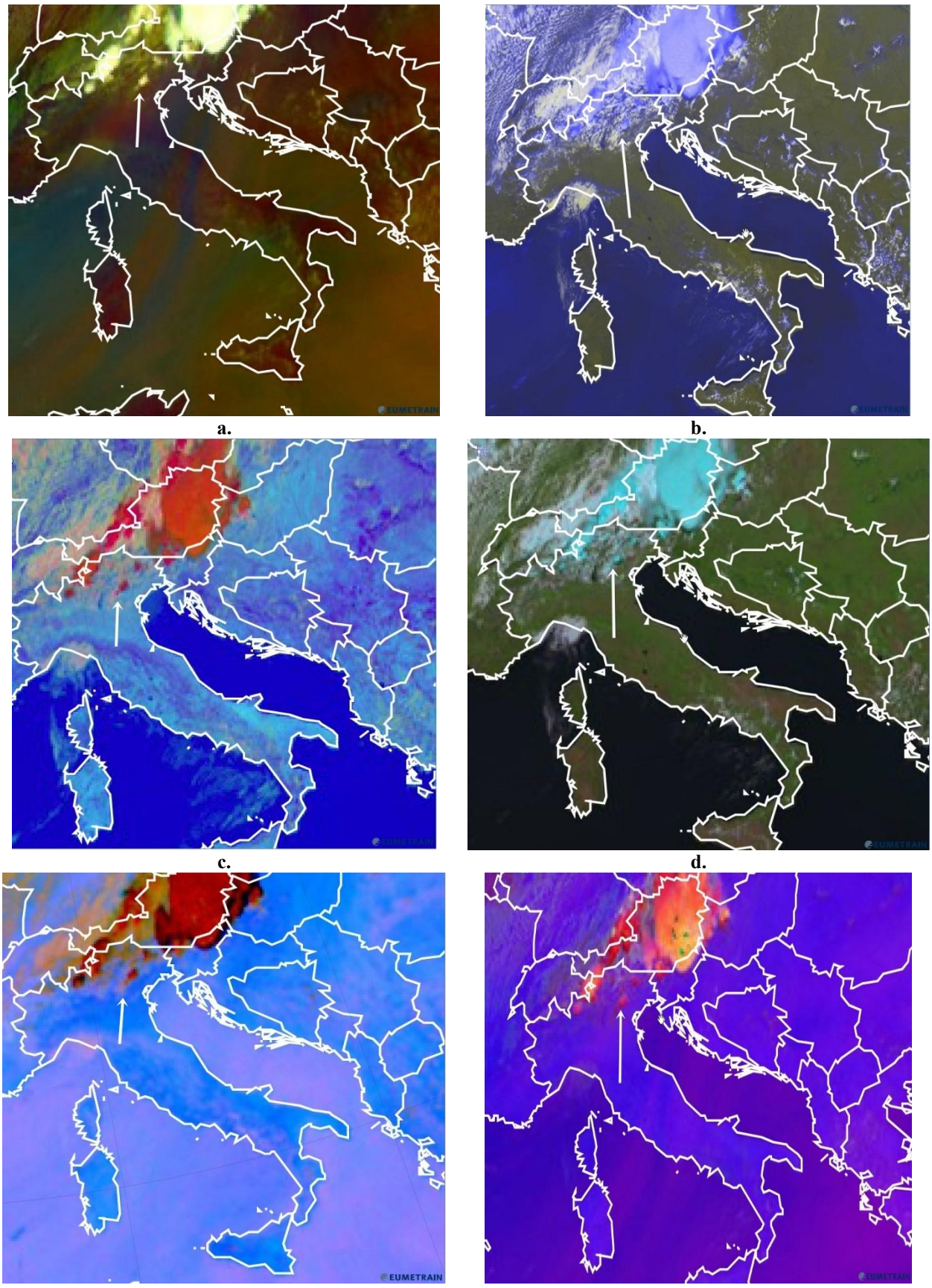

Figure 7. Airmass, Dust, HRVIS, Natural Colour, and Severe Storm RGB composites (R = WV6.2 – WV7.3; G = IR9.7 – IR10.8; B = WV6.2) over the broader Apennine Peninsula, with a white arrow indicating the position of the supercellular storm system, at 12 UTC on 8 July 2015.

According to the ARPAV operational report, total accumulated precipitation across the Veneto region ranged from 20 - 70 mm/24 h, with the highest totals (50 - 70 mm/24 h) recorded along the Vicenza-Treviso provincial boundary. At 09:30 UTC (Figure 8 – up), the BASE Section Corrected Intensity product shows a convective echo over northern Vicenza with reflectivity values of 40 - 60 dBZ concentrated within the core of the developing cell. The echo structure is consistent with the early stages of supercell organization.

By 14:20 UTC, the PPI 1.5° imagery (Figure 9) indicates substantial growth and horizontal expansion of the supercell, driven by strong vertical wind shear and pronounced southwesterly flow aloft with a weaker westerly component. The corresponding vertical cross-section (A-B) shows a storm top exceeding 15 km and a horizontal extent of approximately 42 km. A zone of high reflectivity (~60 dBZ) extends from the cloud base (>1 km) up to nearly 10 km altitude. A strong updraft is evident, although a weak echo region has not yet fully developed at this stage.

At 14:40 UTC, the convective system expands further and intensifies (Figure 10). The vertical cross-section reveals a convective core exceeding 10 km in height with reflectivities near 60 dBZ. A weak echo region becomes apparent, and the updraft zone displays a pronounced local reflectivity minimum, indicative of vigorous vertical velocities.

By 15:20 UTC, the vertical cross-section (Figure 11) shows a clearly developed and strongly expressed bounded weak echo region between 4 - 5 km altitude, along with a continuous updraft column extending from the cloud base (~1 km) to 15 km. The bounded weak echo region occurs when the updraft is sufficiently strong to prevent precipitation from falling through it. Within the gradient zone between high and low reflectivity (near 60 dBZ), the storm exhibits rotation around a vertical axis, forming a mesocyclone between 1 - 5 km altitude. This mesocyclone ultimately generated the tornado.

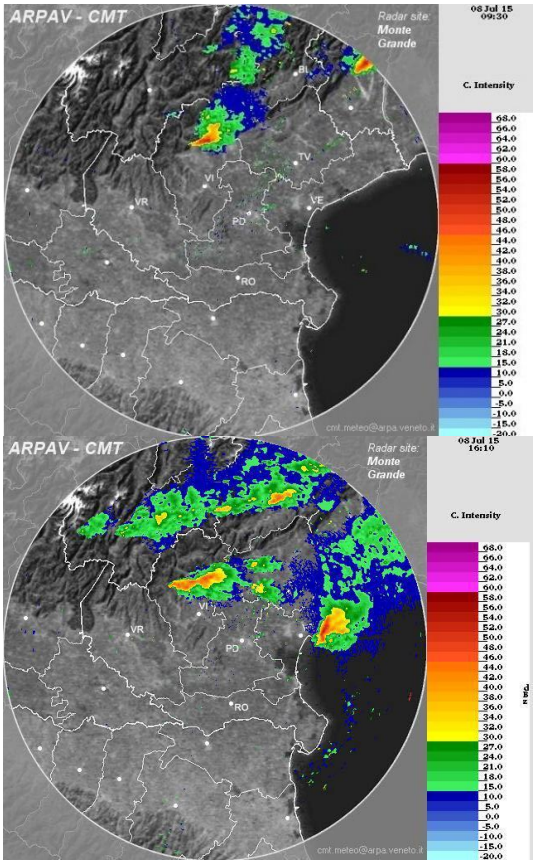

Figure 8. BASE Section Corrected Intensity (dBZ) at 09:30 (up) and 16:10 UTC (down), 8 July 2015, showing the early development of the supercell over northern Vicenza, Veneto region.

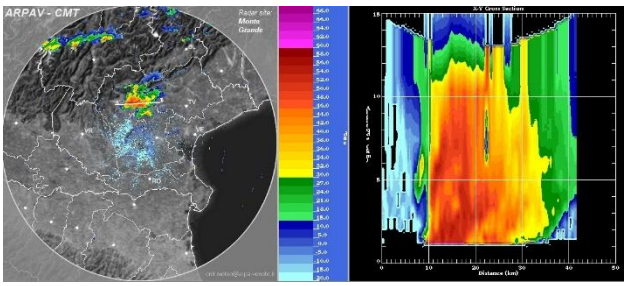

Figure 9. PPI 1.5° Corrected Intensity (dBZ) and vertical cross-section (A-B) of the supercell at 14:20 UTC, 8 July 2015, illustrating horizontal expansion of the supercell and the initial development of a vertical updraft.

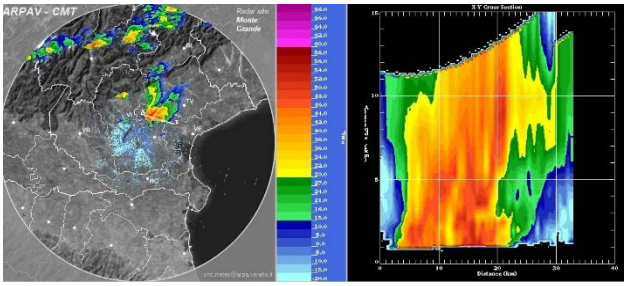

Figure 10. PPI 1.5° Corrected Intensity (dBZ) and vertical cross-section (A-B) of the supercell at 14:40 UTC, 8 July 2015, showing a convective core exceeding 10 km height and the formation of a weak echo region.

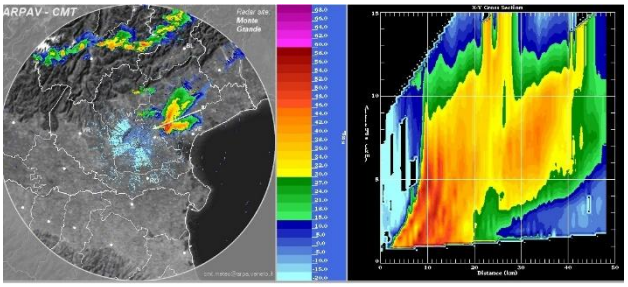

Figure 11. PPI 1.5° radar reflectivity and vertical cross-section (A-B) of the supercell at 15:20 UTC, 8 July 2015, displaying a clearly defined bounded weak echo region from 4 - 5 km altitude and a strong continuous updraft column.

The radar image at 16:10 UTC (Figure 8 - down) reveals a pronounced hook echo (a classic radar signature of mesocyclones, indicates rotating storm cores that can produce tornadoes), marking the final mature stage of the supercell and the tornadic circulation as it moved toward the Gulf of Trieste and the northern Adriatic Sea.

3.6. Ground Survey and *EF*-Scale Forensic Damage Analysis

On 8 July 2015, a powerful supercell thunderstorm (Figure 12a-d), accompanied by heavy precipitation (50 - 70 mm of rainfall) and large hail, affected the Veneto region in northern Italy in the late afternoon (15:30 UTC / 17:30 CET), producing a violent tornado. The tornado propagated across the region along a southwesterly upper-level flow with a slight westerly component. Given the preceding heatwave that had impacted Italy, this severe weather event was anticipated and relatively well forecasted.

ESTOFEX issued a level 2 severe weather forecast for 8 July 2015, indicating a 15% probability of severe convective storms over northern Italy, southern Austria, and Slovenia, primarily for large hail, damaging wind gusts, excessive rainfall, and, to a lesser extent, tornadoes. According to the European Severe Weather Database (ESWD, http://www.eswd.eu), on 8 July 2015, large hail was reported in Thiene (45.71° N, 11.48° E, 147 m AMSL) and Breganze (45.71° N, 11.57° E, 110 m AMSL), while a tornado was recorded in Mira (45.43° N, 12.12° E, 6 m AMSL).

The tornado caused substantial damage in the Veneto region. An 18th-century historic town was completely destroyed, several houses suffered severe structural damage, walls were collapsed, some roofs were removed entirely, and other buildings sustained minor to significant roof damage. While the historical center of Venice remained largely unaffected, a few islands in the lagoon were struck, uprooting trees, destroying roofs, and displacing boats, including several iconic gondolas accumulated on Sant'Elena Island. In total, the tornado impacted 118 islands within the lagoon. Sant'Erasmo Island, at the entrance to the Adriatic Sea, experienced the greatest damage. Agricultural land, intense rainfall, and wind gusts resulted in losses valued at several million euros. A medieval cluster of buildings and approximately 1,000 trees were destroyed on Certosa Island. The tornado continued northeast toward Cavallino, Jesolo, and Eraclea (Figure 13).

On 7 July 2015, the ARPAV Meteorological Service issued weather warnings (CFD) for 8 July, forecasting diffuse and organized convective

a.

b.

c.

d.

Figure 12 (a-d). Supercell thunderstorm with a visible mesocyclone and associated cloud features, including a Cb arcus, wall cloud, beaver tail cloud, and funnel cloud.

phenomena in the late afternoon and evening, initially over the pre-alpine and subalpine areas, and then across the central and northern plains. Observations confirmed an unstable weather phase with the

potential for strong and localized convective events, including heavy showers, strong wind gusts, and hail. Due to the highly localized and unpredictable nature of tornadoes, direct wind speed measurements were not possible. Therefore, the Enhanced Fujita (*EF*) scale provides the most suitable method for forensic wind assessment.

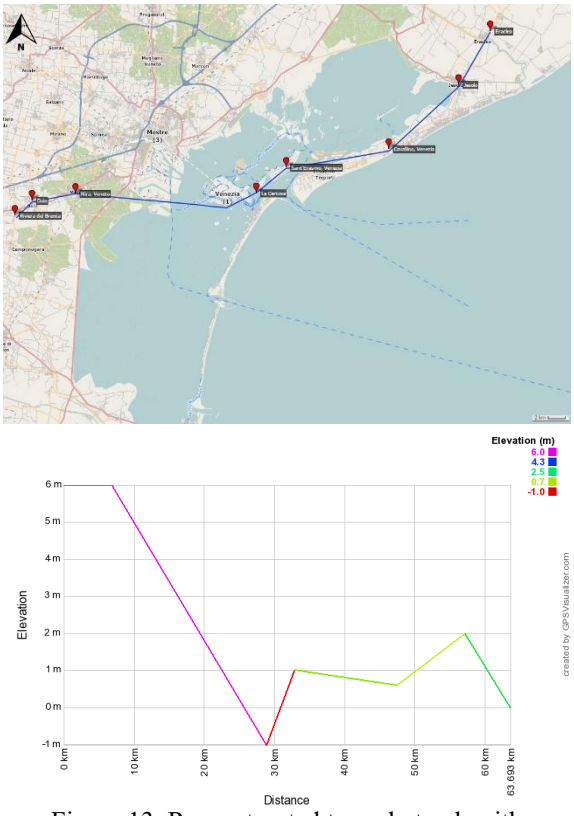

Figure 13. Reconstructed tornado track with corresponding terrain elevation profile along the path.

Based on the conducted damage survey and analysis, the tornado is classified as an *EF4* event. While the brick walls in Mira were bonded with older mortar, which prevented classification as *EF5*, several key characteristics of this *EF4* tornado were recorded in the preliminary report updated on 14 July 2015: the tornado track length was 11.5 km, with a typical path width of 700 m and a maximum width of 1,000 m, reaching a peak intensity of *EF4* on the Enhanced Fujita scale.

4. DISCUSSION

Several studies focusing on Southern Europe and Northern Italy have highlighted the importance of Alpine orography, land–sea contrasts, and mesoscale boundaries in modulating convective evolution and tornadogenesis (Romero et al., 2018; Picca et al., 2010; Delobbe et al., 2013). Our findings are consistent with these results, particularly regarding the deformation and slowing of frontal systems near the Alpine barrier and the enhancement of low-level cyclonic vorticity over the Po Valley and Veneto region. However, the 8 July 2015 event stands out due to the rare intensity of the tornado (*EF4*), placing it among the most severe tornadoes documented in the Mediterranean region.

Compared with previous Mediterranean case studies, which often focus on either synoptic-scale conditions or damage-based assessments, the present work provides an integrated, multi-method reconstruction combining reanalysis data, radiosonde observations, satellite-derived diagnostics, Doppler radar signatures, and post-event damage assessment. This approach allows for a more complete linkage between large-scale atmospheric forcing, mesoscale storm dynamics, and observed tornado intensity. In this respect, the study complements and extends earlier European analyses by explicitly connecting environmental parameters (e.g., wind shear, instability indices, vorticity advection) with radar-observed supercell evolution and tornado formation (Brooks et al., 2003; Doswell et al., 1996; Markowski & Richardson, 2010).

Furthermore, the results reinforce recent findings that strong Mediterranean tornadoes, although rare, are not anomalous when a favorable overlap of thermodynamic instability, vertical wind shear, and upper-level jet dynamics occurs (Antonescu et al., 2016; Miglietta & Matsangouras, 2018). The present case therefore contributes to a growing body of evidence that parts of Northern Italy represent a non-negligible tornado risk zone under specific atmospheric configurations, with direct implications for hazard assessment and environmental risk management in densely populated regions.

While many previously documented Mediterranean tornadoes were associated with weaker intensity or short-lived vortices (Antonescu et al., 2018; Delobbe et al., 2013), the 8 July 2015 Veneto tornado exhibited characteristics typically associated with high-end supercell tornadoes, including a long-lived mesocyclone, pronounced WER/BWER signatures (WER – Weak Echo Region, and BWER – Bounded Weak Echo Region, are radar features indicating strong rotating updrafts in supercell storms), and sustained rotation through a deep layer of the troposphere. In this respect, the event more closely resembles environments documented in classical severe-convection studies from North America (Doswell et al., 2002; Markowski & Richardson, 2014), demonstrating that analogous dynamical processes can occasionally occur in the Mediterranean basin.

The atmospheric structure analysis demonstrates that on 8 July 2015, both thermodynamic and dynamic conditions were highly favorable for the development of a supercell, creating an optimal environment for tornadogenesis in the Veneto region of Northern Italy. The European Severe Weather Database (ESWD) recorded the occurrence of large hail and a tornado in Mira, while ESTOFEX issued a Level 2 severe weather warning for the region. The maximum tornado intensity was estimated as *EF4*, resulting in two fatalities, approximately 20 injuries, and material damage amounting to several million euros. This event raises a fundamental question: whether such a violent tornado represents a statistical anomaly in Southern Europe or a direct manifestation of exceptionally favorable atmospheric conditions (Doswell et al., 1996; Brooks et al., 2003; Trapp et al., 2007; Antonescu et al., 2016).

The results strongly support the latter interpretation. Crucial contributing factors include the Alpine orography, which deformed and decelerated the advancing frontal system, and the presence of a pronounced upper-level jet stream at 300 mb, generating a persistent divergent flow aloft (Bluestein, 1993; Markowski & Richardson, 2010; Romero et al., 2018). Cold-air advection and flow deflection around the Alpine barrier enhanced low-level pressure gradients and cyclonic vorticity, leading to the development of quasi-closed cyclonic circulations over the Veneto region (Johns & Doswell, 1992; Doswell & Burgess, 1993; Picca et al., 2010). These findings are consistent with previous European studies emphasizing the importance of orographic modulation in Mediterranean severe convection (Delobbe et al., 2013; Miglietta & Matsangouras, 2018).

Sounding and mesoscale analyses revealed strong vertical and directional wind shear throughout the troposphere, a key prerequisite for supercell organization and longevity (Weisman & Klemp, 1982; Rasmussen & Blanchard, 1998; Brooks et al., 2003). Divergence in the upper troposphere induced low-level convergence, and when the supercell mesocyclone interacted with these near-surface convergence zones, conditions became favorable for tornado funnel development (Davies-Jones et al., 1990; Thompson et al., 2003; Markowski & Richardson, 2014). Vorticity advection at both 850 and 500 mb provided sufficient dynamical support for sustained storm rotation, reinforcing mesocyclonic development (Doswell et al., 1996; Markowski et al., 1998).

Thermodynamically, high convective instability (MLCAPE exceeding 2000 J kg^{-1}) combined with steep mid-level lapse rates from approximately 700 mb upward enhanced buoyancy and updraft strength (Doswell & Brooks, 1996; Markowski & Richardson, 2010). Multiple stability and instability indices (LI, SI, MTI, TT, KO, and SWISS 12) consistently indicated the potential for intense, localized convective storms (Johns & Doswell, 1992; Thompson et al., 2002). In particular, elevated values of the Supercell Composite Parameter (SCP) and Significant Tornado Parameter (STP) highlighted an enhanced likelihood of tornadic supercells, consistent with environments known to support strong tornadoes (Davies-Jones, 1993; Stensrud et al., 1997; Thompson et al., 2003).

Satellite observations from METEOSAT provided a 'top-down' view of the storm, showing very high, dense clouds containing ice, which indicate strong upward air motion (updrafts) essential for supercell development (Bedka et al., 2010; Bendix & Strübing, 2003). Concurrent ARPAV radar analysis identified a hook echo, a spiral-like radar signature indicative of storm rotation, and a well-defined supercell mesocyclone, a rotating updraft at the storm's core. The radar also showed WER and BWER, which are features associated with strong upward motion and rotation, supporting tornado formation. Cloud tops exceeded 15 km, while reflectivity values surpassed 60 dBz within the convective core, consistent with large hail production and intense downdrafts (Burgess et al., 1982; Bluestein & Parks, 1983; Markowski & Richardson, 2014). Within sharp gradients of radar reflectivity, the storm exhibited rotation about its vertical axis, culminating in tornado formation.

The geographic position and topographic configuration of the Veneto region, combined with the observed atmospheric forcing, were therefore decisive in enabling tornadogenesis. The environmental setup closely resembles the canonical "ingredients-based" framework originally developed for the U.S. Great Plains, including: (1) warm, moist low-level air; (2) warm, dry mid-level air; (3) intrusions of colder air from higher latitudes; (4) a cyclonic pressure field with associated frontal systems; and (5) strong jet-stream support (Bluestein, 1999; Davies-Jones et al., 2001; Doswell et al., 2006). This case demonstrates that, under suitable synoptic and mesoscale conditions, the Mediterranean environment can transiently approximate these canonical settings.

5. CONCLUSION

From a hazard and risk perspective, the findings emphasize that areas downstream of major orographic barriers – particularly the Alpine-Po Valley interface – should be prioritized in regional

tornado hazard mapping. Moreover, the identification of mesoscale precursors such as enhanced low-level shear, upper-level divergence, and radar-detected mesocyclones has direct relevance for early-warning systems in densely populated Mediterranean plains. Although tornadoes remain relatively infrequent in Southern Europe, their potential severity and societal impact necessitate their inclusion in environmental risk assessments, civil protection planning, and resilience strategies, especially in regions characterized by high population density and cultural heritage assets (Dotzek et al., 2003; Holzer et al., 2011; Antonescu et al., 2018).

In conclusion, the exceptional combination of thermodynamic instability, strong vertical wind shear, Alpine orographic forcing, and jet-stream dynamics created a highly conducive environment for an *EF4* tornado in Northern Italy. This study underscores the value of integrated, high-resolution case analyses for improving the understanding of rare but high-impact tornadoes in Europe, thereby supporting more effective hazard assessment, early-warning development, and long-term risk mitigation strategies (Doswell et al., 2002; Markowski, 2002; Miglietta & Matsangouras, 2018).

Figure Sources and Authorship

Figures 5 and 13 were created by the authors using meteorological data and verified sources as indicated in Table 1. Figures 12a, b, and d are ©Valentina Abinanti, www.tornadoseeker.com, and Figure 12c is from https://www.zenastormchaser.it. All other figures were generated or adapted from publicly available meteorological datasets (e.g., radar, satellite, and reanalysis data) with proper attribution in the captions. This statement ensures transparency and proper credit for all visual material included in the manuscript.

REFERENCES

Antonescu, B., Holzer, A. & Schultz, D.M., 2018. *Tornado climatology in Europe*. Quarterly Journal of the Royal Meteorological Society, 144(710), 517–534.

Antonescu, B. & Schultz, D.M., 2016. *Tornadoes in Europe: Synthesis of knowledge and perspectives.* Space Science Reviews, 204, 325–350, https://doi.org/10.1007/s11214-016-0296-3.

Antonescu, B., Schultz, D.M. & Holzer, A., 2016. *European severe convective storm climatology.* Atmospheric Research, 178–179, 1–16.

Avolio, E. & Miglietta, M.M., 2023. *Mediterranean tornado hotspots: Climatology, drivers and implications*. Atmospheric Research, 289, 106865.

Bagaglini, L., Ingrosso, G. & Miglietta, M.M., 2021. *Synoptic and mesoscale analysis of Mediterranean tornado events*. Natural Hazards, 108, 231–251.

Bedka, K.M., Brunner, J.C., Dworak, R., Feltz, W., Otkin, J.A. & Greenwald, T., 2010. *Objective satellite-based detection of overshooting tops using infrared window channel brightness temperature gradients.* Journal of Applied Meteorology and Climatology, 49(2), 181–202, https://doi.org/10.1175/2009JAMC2286.1.

Bendix, J. & Strübing, M., 2003. *Satellite-based analysis of mesoscale convective systems*. Meteorologische Zeitschrift, 12, 277–288.

Bluestein, H.B., 1993. *Synoptic-Dynamic Meteorology in Midlatitudes*. Vol. II. Oxford University Press.

Bluestein, H.B., 1999. *A history of severe-storm-intercept field programs*. Weather and Forecasting, 14(4), 558–577, https://doi.org/10.1175/1520-0434(1999)014<0558>2.0.CO;2.

Bluestein, H.B. & Parks, G.S., 1983. *A synoptic and photographic climatology of low-precipitation severe thunderstorms in the Southern Plains.* Monthly Weather Review, 111(10), 2034–2046, https://doi.org/10.1175/1520 0493(1983)111.

Brooks, H.E., Lee, J.W. & Craven, J.P., 2003. *The spatial distribution of severe thunderstorm and tornado environments from global reanalysis data*. Atmospheric Research, 67–68, 73–94.

Burgess, D.W., Lemon, L.R. & Brown, R.A., 1982. *Mesocyclone evolution statistics.* Preprints, 12th Conference on Severe Local Storms, American Meteorological Society, 422–424.

Davies-Jones, R.P., 1993. *Helicity trends in tornadic thunderstorms.* Journal of the Atmospheric Sciences, 50(24), 4117–4132, https://doi.org/10.1175/1520-0469(1993)050.

Davies-Jones, R.P., Burgess, D.W. & Foster, M.P., 1990. *Test of helicity as a tornado forecast parameter.* Preprints, 16th Conference on Severe Local Storms, American Meteorological Society, 588–592.

Davies-Jones, R.P., Trapp, R.J. & Bluestein, H.B., 2001. *Tornadoes and tornadic storms.* In Severe Convective Storms, Meteorological Monographs, 28(50), 167–221, American Meteorological Society, https://doi.org/10.1175/0065-9401-28.50.167.

Delobbe, L., Holleman, I. & Pinty, J.-P., 2013. *Tornado occurrence in southern Europe*. Natural Hazards and Earth System Sciences, 13, 2861–2875.

Doswell, C.A. & Brooks, H.E., 1996. *The role of instability and shear in severe thunderstorm forecasting.* In Preprints, 18th Conference on Severe Local Storms, American Meteorological Society, 556–560.

Doswell, C.A., Brooks, H.E. & Kay, M.P., 2002. *Climatological estimates of daily tornado probability in the United States.* Weather and Forecasting, 17(4), 640–656, https://doi.org/10.1175/1520-0434(2002)017.

Doswell, C.A., Brooks, H.E. & Kay, M.P., 2006. *Climatological estimates of daily local nontornadic severe thunderstorm probability.* Weather and Forecasting, 21(3), 393–407, https://doi.org/10.1175/WAF930.1.

Doswell, C.A., Brooks, H.E. & Maddox, R.A., 1996. *Flash flood forecasting: An ingredients-based methodology.* Weather and Forecasting, 11(4), 560–581, https://doi.org/10.1175/1520-0434(1996)011.

Doswell, C.A. & Burgess, D.W., 1993. *Tornadoes and tornadic storms.* Severe Convective Storms, Meteor. Monogr., 50, 167–221.

Dotzek, N., Feuerstein, B. & Groenemeijer, P., 2003. *Tornadoes in Europe: Historical review.* Atmospheric Research, 67–68, 163–173.

ECSS, 2017. *European Severe Storms Database*. Available at http://www.essd.eu.

Giaiotti, D.B., Giovannoni, M., Pucillo, A. & Stel, F., 2007. *The climatology of tornadoes and waterspouts in Italy.* Atmospheric Research, 83(2–4), 534–541, https://doi.org/10.1016/j.atmosres.2005.08.020.

Holzer, A.M., Antonescu, B. & Schultz, D.M., 2011. *Tornado risk in Europe.* Bulletin of the American Meteorological Society, 92, 1087–1101.

Johns, R.H. & Doswell, C.A., 1992. *Severe local storms forecasting.* Meteor. Monogr., 50, 223–262.

Markowski, P.M., 2002. *Hook echoes and the rear-flank downdraft.* Monthly Weather Review, 130(4), 852–876, https://doi.org/10.1175/1520-0493(2002)130.

Markowski, P. & Richardson, Y., 2010. *Mesoscale Meteorology in Midlatitudes.* Wiley-Blackwell.

Markowski, P. & Richardson, Y., 2014. *The dynamics of tornadoes and tornadic thunderstorms.* Annual Review of Fluid Mechanics, 46, 45–70, https://doi.org/10.1146/annurev-fluid-010313-141421.

Markowski, P.M., Straka, J.M., Rasmussen, E.N., Blanchard, D.O. & Richardson, Y.P., 1998. *Variability of storm-relative helicity during VORTEX.* Monthly Weather Review, 126(11), 2959–2971, https://doi.org/10.1175/1520-0493(1998)126.

Miglietta, M.M. & Matsangouras, I.T., 2018. *Tornadoes and waterspouts in Italy: Climatology and synoptic conditions.* Atmospheric Research, 213, 36–49.

Picca, P., Homar, V. & Ramis, C., 2010. *Tornadoes in the Mediterranean: A case study approach.* Natural Hazards, 53, 39–53.

Pipinato, L., 2018. *The Tromba del Montello of 24 July 1930: A historical tornado in northeastern Italy.* International Journal of Disaster Risk Reduction, 31, 1202–1213.

Rasmussen, E.N.& Blanchard, D.O., 1998. *A baseline climatology of sounding-derived supercell and tornado forecast parameters.* Weather and Forecasting, 13, 1148–1164.

Romero, R., Ramis, C. & Homar, V., 2018. *Tornadic storms in Northern Italy: Environmental conditions and synoptic analysis.* Atmosphere, 9, 347.

Stensrud, D.J., Cortinas, J.V. & Brooks, H.E., 1997. *Discriminating between tornadic and nontornadic thunderstorms using mesoscale model output.* Weather and Forecasting, 12(4), 613–632, https://doi.org/10.1175/1520-0434(1997)012.

Thompson, R.L., Edwards, R. & Mead, C.M., 2002. *An update to the supercell composite and significant tornado parameters.* Preprints, 21st Conference on Severe Local Storms, American Meteorological Society.

Thompson, R.L., Edwards, R., Hart, J.A., Elmore, K. L. & Markowski, P., 2003. *Close proximity soundings within supercell environments obtained from the Rapid Update Cycle.* Weather and Forecasting, 18(6), 1243–1261, https://doi.org/10.1175/1520-0434(2003)018.

Trapp, R.J., Diffenbaugh, N.S. & Brooks, H.E., 2007. *Severe convective storms in Europe.* Journal of Climate, 20, 4956–4972.

Tsanis, I.K., Kaleris, V. & Bartzis, J.G., 2003. *Mediterranean tornadoes and impacts on urban areas.* Natural Hazards, 28, 33–49.

Weisman, M.L. & Klemp, J.B., 1982. *The dependence of numerically simulated convective storms on vertical wind shear and buoyancy.* Monthly Weather Review, 110, 504–520.

Zanini, D., Hofer, M., Faleschini, F. & Pellegrino, G., 2017. *Structural damage assessment of Italian buildings under tornado wind loading.* Natural Hazards and Earth System Sciences, 17, 1091–1106.

Received: 14. 12. 2025
Revised: 19. 01. 2026
Accepted: 24. 01. 2026
Published online: 26. 01. 2026